PDF (200 K)   Export citation   E-mail article

Thumbnails | Full-Size images

Article   Figures/Tables   References

Boundary element analysis of stress intensity factor K_I in some two-dimensional dynamic thermoelastic problems

P. Hosseini-Tehrani 🖂, **A.R. Hosseini-Godarzi, M. Tavangar**

Automotive Engineering Department, Iran University of Science and Technology, Tehran, Iran

Abstract

This paper presents a numerical technique for the calculation of stress intensity factor as a function of time for coupled thermoelastic problems. In this task, effect of inertia term considering coupled theory of thermoelasticity is investigated and its importance is shown.

A boundary element method using Laplace transform in time-domain is developed for the analysis of fracture mechanic considering dynamic coupled thermoelasticity problems in two-dimensional finite domain. The Laplace transform method is applied to the time-domain and the resulting equations in the transformed

field are discretized using boundary element method. Actual physical quantities in time-domain is obtained, using the numerical inversion of the Laplace transform method.

The singular behavior of the temperature and stress fields in the vicinity of the crack tip is modeled by quarter-point elements. Thermal dynamic stress intensity factor for mode *I* is evaluated using *J*-integral method. By using *J*-integral method effects of inertia term and other terms such as strain energy on stress intensity factor may be investigated separately and their importance may be shown. The accuracy of the method is investigated through comparison of the results with the available data in literature.

Keywords: Dynamic fracture mechanics; Coupled thermoelasticity; Boundary element; Laplace transform

Nomenclature

E	modulus of elasticity
$C_s = \sqrt{(\lambda + 2\mu)/\rho}$	velocity of the longitudinal stress wave
$C = T_0 \gamma^2 / \rho c e (\lambda + 2\mu)$	coupling parameter
c_e	specific heat at constant strain
n_j	a components of outward normal vector to the boundary
k	thermal conductivity
K_I	mode *I* stress intensity factor
$\bar{q}_n$	heat flux vector on the boundary
s	Laplace transform parameter
T	temperature
T_0	reference temperature
$\bar{T}$	temperature on the boundary
t	time
u_i	components of displacement vector
V_{ik}^T	fundamental solution tensor
$(\cdot)$	time differentiation
$(,i)$	partial differentiation with respect to x_i ($i=1,2$)
$\alpha = k/(\rho c_e C_s)$	unit length
γ	stress temperature modulus
λ, μ	Lame's constants
u	Poisson ratio
ρ	mass density

ε_{ij}	the components of strain tensor
σ_{ij}	the components of stress tensor
$\bar{T}_i$	traction vector on the boundary

Article Outline

1. Introduction

In recent years, there has been a great interest in the distribution of thermal stress near to the vicinity of a crack in the interior of an elastic solid, mainly because of its importance in theories of brittle and ductile fracture and many potential applications in industrial facilities. In sensitive equipment such as pressure vessels, the fracture of a component, due to sudden cooling, say, can lead to complete failure. The possibility of a crack-induced failure following thermal shock may be assessed by calculating the thermal stress intensity factors for the cracked component.

Just now there is no report on the evaluation of the dynamic stress intensity factor for thermal shock problems with the coupled thermoelastic assumption with the inertia term. The previous works are limited to evaluate the stress intensity factor and/or the thermal shock stress intensity factor for transient or coupled thermoelasticity problems where the inertia term is ignored.

In the classical study of thermoelastic crack problems, the theoretical solutions are available only for very few problems in which cracks are contained in infinite media under special thermal loading conditions, such as in the work of Kassir and Bergman [1]. For cracked bodies of finite dimensions, exact solutions are impossible to obtain. Wilson and Yu [2] employed the finite element method to deal with these problems. The method is combined with the modified *J*-integral theory proposed by them. The other prevailing methods employed by Nied [3] and Chen and Weng [4] is based on the concept of principle superposition. That is, in the absence of a crack, the thermal loading is replaced by a traction force, which is equivalent to the internal force at the prospective crack face.

Uncoupled transient thermoelasticity has been the subject of many investigations with a boundary element method of analysis. For instance, Tanaka et al. [5] implemented a volume based thermal body approach. However, volume discretization removes some of the advantages of the standard BEM. Sladek and Sladek [6] presented a series of papers on coupled thermoelasticity that included a time-domain method. The initial time-domain boundary integral equation, were presented in a boundary only formulation, but the primary variables include time derivatives. Sladek and Sladek [7] later presented a boundary integral formulation in terms of regular primary variables; they used inverse Laplace transforms on their previous equations. Raveendra et al. [8] also used a sub region technique to solve crack problems using a boundary only

formulation. Hosseini-Tehrani et al. [9] presented a boundary element formulation for dynamic crack analysis considering coupled theory of thermoelasticity. In this article using crack opening displacement method, conditions where the inertia term plays an important role is discussed as well as the effects of coupling parameter on crack intensity factor variations.

This paper presents a boundary element formulation for the crack analysis considering coupled theory of thermoelasticity. In this work an isotropic and homogeneous material, in two-dimensional plain strain geometry with an initial edge crack on its boundary is considered. The body is exposed to a thermal shock on its boundary and the resulting thermal stress waves are investigated through the coupled thermoelastic equations. Due to the short time interval of the imposed thermal shock, the Laplace transforms method is employed to model the time variable in the boundary element formulation. The discretized forms of the equations are obtained by the approximation of boundary variations by quadratic elements, and the quarter point singular element is used at the crack tip. The present approach is used to evaluate the thermal dynamic stress intensity factor (TDSIF) at the first opening crack mode. An infinite strip with a crack on its surface under sudden cooling is considered. TDSIF is obtained using *J*-integral method. For thermal shock loading, the time dependent TDSIF is obtained using the Durbin [10] method. The results are compared with the available transient results. Effects of different terms such as strain energy and, inertia term on crack intensity factor are discussed using coupled and uncoupled theories of thermoelasticity.

2. Governing equations

A homogeneous isotropic thermoelastic solid is considered. In the absence of body forces and heat generation, the governing equations for coupled theory of thermoelasticity in time-domain are:

$$(\lambda + \mu)u_{j,ij} + \mu u_{i,jj} - \gamma T_{,i} - \rho \ddot{u}_i = 0 \tag{1}$$

$$kT_{,ii} - \rho c_e \dot{T} - \gamma T_0 \dot{u}_{j,j} = 0 \tag{2}$$

The dimensionless variables are defined as:

$$\hat{x} = \frac{x}{\alpha}, \quad \hat{t} = \frac{tC_s}{\alpha}, \quad \hat{\sigma}_{ij} = \frac{\sigma_{ij}}{\gamma T_0}, \tag{3}$$

$$\hat{u}_i = \frac{(\gamma + 2\mu)u_i}{\alpha \gamma T_0}, \quad \hat{T} = \frac{T - T_0}{T_0}$$

Eqs. (1) and (2) takes the form (dropping the hat for convenience):

$$\frac{\mu}{\lambda + 2\mu}u_{i,jj} + \frac{\lambda + \mu}{\lambda + 2\mu}u_{j,ij} - T_{,i} - \ddot{u}_i = 0 \tag{4}$$

$$T_{,ii} - \dot{T} - \frac{T_0\gamma^2}{\rho c_e(\lambda + 2\mu)}\dot{u}_{j,j} = 0 \tag{5}$$

Transferring Eqs. (4) and (5) to the Laplace domain yields:

$$\frac{\mu}{\lambda + 2\mu}\tilde{u}_{i,jj} + \frac{\lambda + \mu}{\lambda + 2\mu}\tilde{u}_{j,ij} - \tilde{T}_{,i} - s^2\tilde{u}_i = 0 \tag{6}$$

$$\bar{T}_{,jj} - s\bar{T} - \frac{T_0\gamma^2}{\rho c_\alpha(\gamma + 2\mu)} s\tilde{u}_{j,j} = 0 \tag{7}$$

Eqs. (6) and (7) can be rewritten in matrix form as

$$L_{ij}\bar{U}_j = 0 \tag{8}$$

where $\bar{U}_j = \{\tilde{u}_1, \tilde{u}_2, \bar{T}\}$. The boundary conditions are assumed to be as follow:

$$u_i = \bar{u}_i \ \ \text{on} \ \Gamma_\alpha \quad \tau_i = \bar{\tau}_i = \sigma_{ij}n_j \ \ \text{on} \ \Gamma_\tau \tag{9}$$

$$T = \bar{T} \ \ \text{on} \ \Gamma_T \quad q = \bar{q}_n = q_i n_i \ \ \text{on} \ \Gamma_q$$

In order to derive the boundary integral problem, the following weak formulation of the differential equation set (8) for the fundamental solution tensor V_{ik}^* is considered:

$$\int_\Omega (L_{ij}U_j)V_{ik}^* \ \mathrm{d}\Omega = 0 \tag{10}$$

After integrating by parts over the domain and taking a limiting procedure approaching the internal source point to the boundary point, the following boundary integral equation is obtained

$$\tag{11}$$

$$C_{kj}U_k(y,s) = \int_\Gamma \left[\tau_\alpha(x,s)V_{\alpha j}^*(x,y,s) - U_\alpha(x,s)\sum_{\alpha j}^*(x,y,s) \right] \mathrm{d}\Gamma(x)$$

$$+ \int_\Gamma [T_{,n}(x,s)V_{3j}^*(x,y,s) - T(x,s)V_{3j,n}^*(x,y,x)]\mathrm{d}\Gamma(x)$$

$$\alpha = 1,2; \qquad j = k = 1,2,3 \quad (11)$$

where C_{kj} denote the shape coefficient tensor. The kernel $\sum_{\alpha j}^*$ in (11) is defined by:

$$\tag{12}$$

$$\sum_{\alpha j}^* = \left[\left(\frac{\lambda}{\lambda + 2\mu}V_{kj,k}^* + \frac{T_0\gamma^2}{\rho c_\alpha(\lambda + 2\mu)}sV_{3j}^* \right)\delta_{\alpha\beta} \right.$$

$$\left. + \frac{\mu}{\lambda + 2\lambda}(V_{\alpha j,\beta}^* + V_{\beta j,\alpha}^*) \right] n_\beta \tag{12}$$

Here the fundamental solution tensor V_{ik}^* must satisfy the differential equation

$$l_{ij}V_{ik}^* = \delta_{ik}\delta(y - x) \tag{13}$$

where l_{ij} is the adjoint operator of $L_{ij}(\mu_{ij}=(l_{ij})^{-1}\det(l_{ij}))$ in Eq. (8).

3. Fundamental solution

In order to construct the fundamental solution, we put the fundamental solution tensor V_{ik}^* of Eq. (13) in the following potential representation using the transposed co-factor operator l_{ij} of μ_{ij} and scalar function Φ^*:

$$V_{ij}^* = \mu_{ij}\Phi^*(x,y,s)$$

(14)

After substituting Eqs. (14) into (13), the following differential equation is obtained

$$\Lambda\Phi^*(x,y,s) = -\delta(x-y)$$

(15)

where the operator Λ is

$$\Lambda = \det(l_{ij}) = \frac{\mu}{\lambda + 2\mu}(\Delta - h_1^2)(\Delta - h_2^2)(\Delta - h_3^2)$$

(16)

and Δ denotes the Laplacian. h_i^2 are the solution of:

(17)

$$h_1^2 = \frac{\lambda}{\lambda + 2\mu}s^2 \quad h_2^2 + h_3^2 = s^2 + s + \frac{T_0\gamma^2}{\rho C_\varepsilon(\lambda + 2\mu)}s$$
$$h_2^2 h_3^2 = s^3$$

(17)

The solution for Φ^* from Eq. (15) with help of Eq. (16) is thus:

(18)

$$\Phi^* = \frac{\lambda + 2\mu}{2\pi\mu}\left[\frac{K_0(h_1 r)}{(h_2^2 - h_1^2)(h_3^2 - h_1^2)} + \frac{K_0(h_2 r)}{(h_1^2 - h_2^2)(h_3^2 - h_2^2)}\right.$$
$$\left. + \frac{K_0(h_3 r)}{(h_1^2 - h_3^2)(h_2^2 - h_3^2)}\right]$$

(18)

The fundamental solution tensor V_{ik}^* for two-dimensional domain is found as follows

$$V_{\alpha\beta}^* = \sum_{k=1}^{3}(\psi_k(r)\delta_{\alpha\beta} - \chi_k r_{,\alpha} r_{,\beta})$$

(19)

$$V_{3\alpha}^* = \sum_{k=1}^{3}\xi_k^I(r)r_{,\alpha} \quad V_{\alpha3}^* = \sum_{k=1}^{3}\xi_k(r)r_{,\alpha}$$

$$V_{33}^* = \sum_{k=1}^{3}\zeta_k(r) \quad \alpha,\beta = 1,2$$

where

(20)

$$\psi_k = \frac{W_k}{2\pi}\left[(h_k^2 - m_2)(h_k^2 - m_1) + \left(\frac{\lambda + \mu}{\mu}\right)\right.$$
$$\left. \times\left(h_k^2 - m_1 - m_1^2 C\frac{\lambda + 2\mu}{\lambda + \mu}\right)h_k^2\right]K_0(h_k r)$$
$$+ \frac{W_k(\lambda + \mu)}{2\pi\mu}\left[h_k^2 - m_1 - m_1^2 C\frac{\lambda + 2\mu}{\lambda + \mu}\right]\frac{h_k}{r}K_1(h_k r)$$

$$\chi_k(r) = \frac{W_k(\lambda + \mu)}{2\pi\mu}\left[h_k^2 - m_1 - m_1^2 C\frac{\lambda + 2\mu}{\lambda + \mu}\right]\frac{h_k}{r}K_2(h_k r)$$

$$\xi_k'(r) = \frac{W_k}{2\pi\mu}m_1(h_k^2 - m_2)h_k K_1(h_k r)$$

$$\xi_k(r) = \frac{W_k}{2\pi\mu}Cm_1(h_k^2 - m_2)h_k K_1(h_k r)$$

$$\zeta_k(r) = \frac{W_k}{2\pi\mu}(h_k^2 - m_2)(h_k^2 - S^2)K_0(h_k r) \qquad (20)$$

and

$$r = \|x - y\|; \quad m_1 = s; \quad m_2 = \frac{\lambda + 2\mu}{\mu}s^2 \qquad (21)$$

$$W_i = \frac{-1}{(h_i^2 - h_j^2)(h_k^2 - h_i^2)}; \quad i = 1,2,3; \; j = 2,3,1;$$

$$k = 3,2,1$$

Here, K_0, K_1 and K_2 are modified Bessel function of second kind zero, first, and second orders, respectively.

In order to solve numerically the boundary element integral Eq. (11), the standard boundary element procedure may be applied. When transformed numerical solutions are specified, transient solutions may be obtained using an appropriate numerical inversion technique. In this paper, a method presented by Durbin [10], which combines the Fourier cosine and sine transform to reduce numerical error, is adopted for the numerical inversion. This formulation yields time-domain functional values $F(t_n)$ as

(22)

$$F(t_n) = \frac{2\,e^{n\beta\Delta t}}{t_N}\left\{-\frac{1}{2}\mathrm{Re}[\bar{F}(s_0)] + \mathrm{Re}\left[\sum_{k=0}^{N-1}(A_k + iB_k)W^{nk}\right]\right\}$$
$$\text{for } n = 0,1,\ldots,N-1 \text{ and } t_n = n\Delta t \qquad (22)$$

where Δt is the time step, $\bar{F}$ is the function in the Laplace domain and

(23)

$$A_k = \sum_{l=0}^{L}\mathrm{Re}[\tilde{F}(s_k + lN)], \quad B_k = \sum_{l=0}^{L}\mathrm{Im}[\tilde{F}(s_k + lN)]$$

$$W = e^{2\pi il/N}, \quad s_m = \frac{\beta + 2\pi im}{t_N} \qquad (23)$$

with the real constant $\beta=6/t_n$ based upon experience and the recommendation of Durbin [10]. Different values of $5\leq\beta t_n\leq10$, according to Durbin's recommendation, were considered in the analysis and verification of the method. The best results were achieved by choosing $\beta t_n=6$. This value was used for all examples given in this paper. Note that form Eqs. (22) and (23), the determination of $F(t_n)$ for $n=0,1,\dots,N-1$ depends upon the values of $\bar{F}(s_m)$ for $m=0,1,\dots,M-1$, where $M=N(L+1)$. Consequently, the boundary integral equations

(24)

$$
C_{kj}U_k(y,s_m) = \int_\Gamma \{\bar{T}_\alpha(x,s_m)V^*_{\alpha j}(x,y,s_m) - \bar{U}_\alpha(x,s_m)
$$
$$
\times \sum^*_{\alpha j}(x,y,s_m)\mathrm{d}\Gamma(x) + \int_\Gamma \{\bar{T}_{,n}(x,s_m)V^*_{3j}(x,y,s_m)
$$
$$
- \tilde{T}(x,s_m)V^*_{3j,n}(x,y,s_m)\}\mathrm{d}\Gamma(x) \quad \alpha = 1,2 \qquad (24)
$$

must be solved independently at each of the M discrete values s_m of the transform parameters. In the current implementation, $N=80$ and, $L=0$ is considered to minimize the computational effort.

4. Numerical formulation

The boundary of the solution domain Γ is divided into N element, such that Eq. (11) becomes

(25)

$$
C_{kj}U_k(y,s) = \sum_{n=1}^{N} \int_{\Gamma_n} \bar{T}_\alpha(x,s)V^*_{\alpha j}(x,y,s) - \bar{U}_\alpha(x,s)
$$
$$
\times \sum^*_{\alpha j}(x,y,s)\mathrm{d}\Gamma_n(x) + \sum_{n=1}^{N} \int_{\Gamma_n} [\bar{T}_{,n}(x,s)V^*_{3j}(x,y,s)
$$
$$
- \tilde{T}(x,s)V^*_{3j,n}(x,y,s)]\mathrm{d}\Gamma_n(x) \qquad (25)
$$

where $\Gamma = \sum_{n=1}^{N}\Gamma_n$. On each element the boundary parameter x (with components x_j), the unknown displacement and temperature field $\bar{U}_j(x,s)$, the traction field $\bar{T}_\alpha(x,s)$ and the heat flux field $\bar{T}_{,n}(x,s)$ are approximated using the interpolation functions in the form

$$
x = \sum_{\theta=1}^{m} M^\theta x^\theta, \quad \bar{U} = \sum_{\theta=1}^{m} N^\theta \bar{U}^\theta, \quad \bar{T} = \sum_{\theta=1}^{m} N^\theta \bar{T}^\theta \qquad (26)
$$

where $M\theta$ and $N\theta$ are called the shape functions and are polynomials of degree $m-1$. The property of these shape functions is such that they are equal to 1 at nod θ and 0 at all other nodes, Here, $x\theta$, $\bar{U}^\theta$ and $\bar{T}^\theta$ are the values of the function at node θ.

The different choices of $M\theta$ and $N\theta$ lead to different boundary element formulation. If $M\theta=N\theta$, the formulation is referred to as isoparametric and, if $M\theta$ is a higher-order polynomial than $N\theta$, then the formulation is referred to as superparametric. Conversely, if $M\theta$ is a lower-order polynomial than $N\theta$, then the formulation is referred to as subparametric.

For the present two-dimensional formulation, the isoparametric element is considered. The shape functions $M\theta$ are defined in terms of the non-dimensional coordinates $\xi(-1\leq\xi\leq1)$ and can be derived from the Lagrange polynomials defined, for degree $m-1$, as:

$$M^{\theta}(\xi) = \prod_{i=0; i \neq \theta}^{m} \frac{\xi - \xi_i}{\xi_{\theta} - \xi_i} \tag{27}$$

It is seen that $M\theta(\xi)$ is given by the product of m linear factors. The Lagrangian shape function $M\theta(\xi)$ can be shown to have the following properties. At node

$$M^{\theta}(\xi_{\beta}) = \delta_{\theta\beta}, \quad \xi_1 \leq \xi_{\beta} \leq \xi_m \tag{28}$$

where $\xi_1 = -1$ is the first and $\xi_m = 1$ is the last point in each element. Also:

$$\sum_{\theta=1}^{m} M^{\theta}(\xi) = 1, \quad \sum_{\theta=1}^{m} \frac{dM^{\theta}(\xi)}{d\xi} = 0 \tag{29}$$

For constant and quadratic elements, the shape functions $M\theta(\xi)$ are listed as follows.

For the constant element, $m=1$ and $M(\xi)=1$. For a quadratic element considering:

$$\tag{30}$$

$$l_1 = \frac{1}{2}(1 - \xi), \quad l_2 = \frac{1}{2}(1 + \xi), \quad M^1(\xi) = l_1(2l_1 - 1),$$
$$M^2(\xi) = 4l_1 l_2, \quad M^3(\xi) = l_2(2l_2 - 1) \tag{30}$$

A discretized boundary element formulation can be obtained by substituting Eqs. (26) and (27) with $M\theta = N\theta$, into the integral Eq. (25) to obtain:

$$\tag{31}$$

$$C_{kj}\bar{U}_k(y, s) + \sum_{n=1}^{N}\sum_{\theta=1}^{m} \bar{U}_k^{n\theta} P_{kj}^{n\theta} = \sum_{n=1}^{N}\sum_{\theta=1}^{m} (\bar{r}_{\alpha}^{n\theta} Q_{\alpha j}^{n\theta} + \bar{T}_n^{n\theta} Q_{3j}^{n\theta}),$$
$$k, j = 1, 2, 3; \quad \alpha = 1, 2 \tag{31}$$

The coefficients $P_{kj}^{n\theta}$ and $Q_{kj}^{n\theta}$ are defined in term of the integrals over Γ_n where $d\Gamma_n(\xi)$ becomes $J^n(\xi)d\xi$. Therefore:

$$P_{\alpha j}^{n\theta} = \int_{-1}^{1} M^{\theta}(\xi) \sum_{\alpha j}^{*}(y, x(\xi), s) J^n(\xi) d\xi, \tag{32}$$

$$P_{3j}^{n\theta} = \int_{-1}^{1} M^{\theta}(\xi) V_{3j,x}^{*}(y, x(\xi), s) J^n(\xi) d\xi,$$

$$Q_{kj}^{n\theta} = \int_{-1}^{1} M^{\theta}(\xi) V_{kj}^{*}(y, x(\xi), s) J^n(\xi) d\xi.$$

In general, the Jacobian $J(\xi)$ of a transformation is given as:

$$J(\xi) = \left[\left(\frac{dx_1}{d\xi} \right)^2 + \left(\frac{dx_2}{d\xi} \right)^2 \right]^{1/2} \tag{33}$$

Therefore:

$$J^n(\xi) = \left\{ \left[\sum_{\theta=1}^{m} \frac{dM^\theta(\xi)}{d\xi} x_1^{n\theta} \right]^2 + \left[\sum_{\theta=1}^{m} \frac{dM^\theta(\xi)}{d\xi} x_2^{n\theta} \right]^2 \right\}^{1/2} \tag{34}$$

5. Evaluation of TDSIF

The magnitude of stress intensity factor is a measure of the severity of the crack in both dynamic and static problems. The stress intensity factor may be determined from the crack-opening displacements formula (Fig. 1), considering two-points displacements on each edge of the crack, the stress intensity factors are given by Blandford et al. [11] as follows

$$K_I \frac{\mu}{\kappa+1} \sqrt{\frac{2\pi}{l}} [4(v_B - v_D) + v_E - v_C] \tag{35}$$

where $\kappa = 3-4v$ for plane strain and $(3-v)/(1+v)$ for plane stress condition and the length of the singular element at the crack tip is represented by l. The points B, C, D and E are shown in Fig. 1, where $AC=l$ and $AB=l/4$.
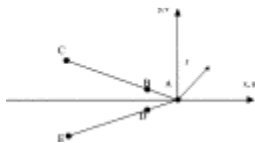
Full-size image (2K)

Fig. 1.

Element geometries for stress intensity factor computations.

For symmetric crack $v_B=-v_D$ and $v_C=-v_E$, and the expression for K_I is simplified to:

$$K_I = \frac{2\mu}{\kappa+1} \sqrt{\frac{2\pi}{l}} (4v_B - v_C) \tag{36}$$

A different formula based on one-point displacement on each edge of the crack is obtained if v_B at $r=l/4$ is considered. This formula is [12]:

$$K_I = \frac{\mu}{\kappa+1} \sqrt{\frac{2\pi}{l}} v_B \tag{37}$$

The dynamic stress intensity factors can also be determined from a path independent J-integral [12], [13], [14] and [15]. For a mixed mode case, the fields of derivatives of displacements, strains, stresses, tractions and accelerations are decomposed into the symmetric mode I and the antisymmetric mode II and the J-integral is calculated for the first mode of deformation as

$$J^I = \int_{S+S_C} (Wn_1 - t_i u_{i,1}) dS + \int_A \rho \ddot{u}_i u_{i,1} \, dA + \int_A \alpha_t \sigma_{ii} T_{,1} \, dA \tag{38}$$

where S is an arbitrary curve surrounding the crack tip; S_C are the crack surfaces; A the area enclosed by S and S_C; W the strain energy density; n_1 the component of the unit outward normal to the boundary of A; and l is the mode of deformation. The elastic strain energy W is given by:

$$W = \int_0^{\varepsilon_{ij}^e} \sigma_{ij} d\varepsilon_{ij}^e \quad \text{where} \quad \varepsilon_{ij}^e = \varepsilon_{ij} - \varepsilon \alpha_t \theta \delta_{ij} \tag{39}$$

The variables in Eq. (38) are expressed in the local crack reference system, shown in Fig. 2. The TDSIFs are calculated from the J^l-integral, as follows:

$$K_I = \sqrt{\frac{8\mu}{\kappa + 1} J^l} \tag{40}$$

Full-size image (13K)
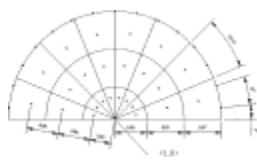
Fig. 2.

Integration path for the J-integral and its discretization. Crack tip is located at (1, 0). All dimensions are normalized dividing by crack length.

The path independent integrals are calculated for a regular polygonal path with the center at the crack tip. The first and last points of the path are the nodes on the crack faces. The discretization of the domain enclosed by the path is shown in Fig. 2. All the variables required for the J-integral are obtained by using the appropriate boundary element equations. The accelerations are calculated by using the displacement at different time steps and the central difference method

$$\ddot{u}_i^N = \frac{1}{\Delta t^2}(u_i^{N-1} - 2u_i^N + u_i^{N+1}) \tag{41}$$

where Δt is the time step and superscripts denote time nodes. The accuracy of the above approximation depends on the variation of accelerations. A better approximation may be obtained by calculating the acceleration directly from the boundary element equation, as has been shown in Fedelinski et al. [16].

The boundary term in Eq. (38) is computed using the trapezoidal rule and the domain term by using Gaussian integration. The centers of trapeziums and triangles which are used for Gaussian integration are shown in Fig. 2.

6. Results and discussion

If the period of thermal shock duration is small enough compared to the first period of natural vibration, then the dynamic thermoelasticity may be important. Consider an infinite strip shown in Fig. 3, initially subjected to a uniform temperature T_0 with an edge crack perpendicular to its top surface The strip is rapidly cooled by conduction at its upper surface $x_2=0$, whereas the bottom surface $x_2=W$ is insulated. This is a mode I crack opening problem. The crack edges assumed to be thermally insulated. Due to the symmetry about the x_2-axis, only half of the strip is discretized.
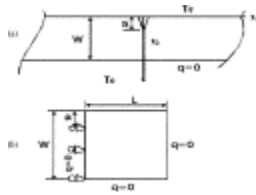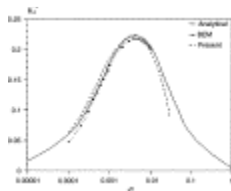
Full-size image (5K)

Fig. 3.

(a) Cracked strip initially at T_0 under sudden cooling T_e and (b) boundary condition.

To solve the problem by boundary element method a proper length to width ratio must be defined. Different ratios of length to width have different effects on maximum stress intensity factor. Katsareas and Anifantis [17] showed that the ratios of $L/W \geq 1$ have minor effect on the maximum stress intensity factor around the crack tip. Therefore, to select a minimum and reliable solution domain and consequently minimum number of boundary elements, $L/W = 1$ is selected. The boundary is divided into 24 quadratic elements. Using larger number of elements did not alter the results by a significant amount. Quarter-point singular elements are used adjacent to the crack tip (in front and behind of the crack tip). The boundary element model is presented in Fig. 3(b), for a crack depth of $a^* = 0.05$ and $L/W = 1$, where $a^* = a/W$. K_I^* is defined as the dimensionless TDSIF, which for plain strain condition is $K_I^* = K_I(1 - v) / \left[\alpha_t E \sqrt{W} (T - T_0) \right]$ and $t^* = kt$ $(/\rho c e W^2)$ is the dimensionless time known as the Fourier number.

In all preceding computations, TDSIF's are obtained using COD one-point displacement formula and, J-integral method. Many investigators such as Boley and Winer [18], Jadeja and Loo [19] indicated that the effect of the inertia term becomes more significant only when parameter B_1, the ratio of the characteristic thermal time $(L^2 \rho c \varepsilon / k)$ to the characteristic mechanical time (proportional to natural period of vibration of the structure), becomes small. This is the condition corresponding to the very thin structures. For the purpose of comparison, B_1 is considered in the order of 10^7, therefore, the effect of inertia term is negligible.

Fig. 4 shows the variation of stress intensity K_I^* versus t^*. The calculations are carried out for a quarter-point crack-tip element using the uncoupled theory of thermoelasticity. In Fig. 4, the variation of K_I^* versus time derived by the analytical method obtained by Lee and Sim [20], the boundary element method [17], and the method described in the present work are compared. The analytical solution of Lee and Sim [20] and the boundary element method solution used by Katsareas and Anifantis [17] are obtained ignoring the inertia term. The analysis of the present work with the assumed B_1 has good agreement with the analytical and boundary element method results.
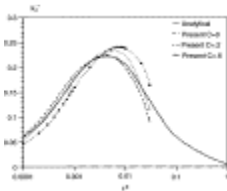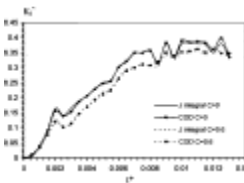

Full-size image (6K)

Fig. 4.

Comparison of the dimensionless thermal dynamic stress intensity factor K_I^* versus dimensionless time t^*, with analytical and numerical transient results.

To study the effect of thermo-mechanical coupling, the variation of K_I^* versus the dimensionless time for different coupling parameters are shown in Fig. 5. As the coupling parameter is increased, the peak value of K_I^* increases. The increase of the coupling parameter, however, causes the peak value of K_I^* occurs at larger time. This is the same result obtained by Chen and Weng [4]. They used coupled thermoelastic equations without consideration of the inertia term.

Full-size image (6K)

Fig. 5.

Comparison of the dimensionless thermal dynamic stress intensity factor K_I^* versus dimensionless time considering coupled theory of thermoelasticity with uncoupled analytical result for different coupling parameters.

Fig. 4 and Fig. 5 are the plot of K_I^* versus time, but the time scale is selected large enough to compare the results with the known data (t^*=1 is of the order of 10 s). To see the effects of the inertia term, however, the time scale must be selected small. To observe the effects of the inertia term, t^*=1 must be in the order of 10^{-11} s (for more details see Hosseini-Tehrani et al. [21]), which is equivalent to 400 times $\hat{t} = 1$.

Fig. 6 shows crack intensity factor variation versus dimensionless time t^*. In this figure, t^*=1 means 9.3×10^{-12} s and W is equal to 40*α.

Full-size image (7K)

Fig. 6.

Comparison of K_I^* variation versus t^* using J-integral and COD methods for uncoupled and coupled theories.

This figure compares K_I^*, obtained by COD and J-integral methods considering uncoupled and coupled theory of thermoelasticity. As it is seen there is no significant difference between these two methods.

In Fig. 6, K_I^* is increased instantaneously after application of sudden cooling. At time t^*=0.002, the thermoelastic wave stress reaches the tip of the crack. This cold shock produces tensile stress in the x_2-

direction and due to the effect of Poisson's ratio; compressive stress produced in the x_1-direction. This phenomenon results in crack opening and thus K_I^* increases by time, as shown in Fig. 6.

When the thermoelastic wave front passes through the crack tip, a compressive stress produced in the x_2-direction and a tensile stress in the x_1-direction in the domain, tensile stress causes extension in the x_1-direction, and while the crack edges are free they can move towards each other. This phenomenon has a decreasing effect on K_I^*. This decrease is shown in Fig. 6 following t^*=0.002 to about t^*=0.0035. From t^*=0.0035, the K_I^* value is increased with a slower rate compared to the initial increase. As time is advanced, the thermoelastic waves are reflected from the boundaries and cause fluctuations in the K_I^* value versus time. The K_I^*-curve for the coupled case of C=0.6 is shown in Fig. 6. This curve is below the K_I^*-curve for the uncoupled case. This result is justified with Fig. 5 for the small values of time.

The J-integral, which represents the dynamic energy release rate for propagating cracks, contains inertia and strain energy terms. J-integral method allows calculating these two terms separately. In this way, the importance of each term may be investigated. Fig. 7 and Fig. 8 show the effects of inertia and strain energy on computed J-integral. Through comparison of strain energy and, J-integral, it seems that fluctuations on J-integral are mainly caused by inertia term. These fluctuations are related to wave reflection from the cracks' tip and boundaries.
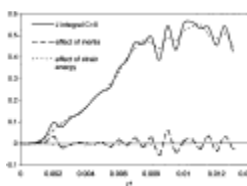
Full-size image (7K)

Fig. 7.

Variation of the J-integral, effect of inertia and strain energy terms versus t^* for uncoupled theory.
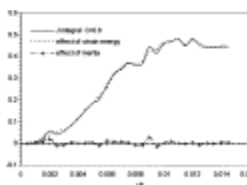
Full-size image (6K)

Fig. 8.

Variation of the J-integral, effect of inertia and strain energy terms versus t^* for coupled theory.

The most important conclusion from these results is this fact: the magnitude of crack intensity factor is mostly dependent on strain energy term. In Fig. 6, Fig. 7 and Fig. 8, the maximum value of K_I^* is nearly two times of the maximum value of K_I^* in Fig. 4. This higher value is achieved because the strain energy and stresses are computed using dynamic thermoelasticity formula, containing inertia term, and considering conditions where this term is important.

7. Conclusions

A boundary element method and Laplace transform in time-domain are developed for the analysis of fractured planar bodies subjected to thermal shock type loads.

The transient coupled thermoelasticity is solved without domain discretization. The singular behavior of the temperature and stress fields, in the vicinity of the crack tip, is modeled by quarter-point elements. The thermal dynamic stress intensity factor for mode I is evaluated from computed nodal values, using the COD and J-integral formulas. The accuracy of the method is investigated through comparison of present results with available analytical and numerical works.

The important results of this study are:

1. Treatment of the time-domain in this paper is through the Laplace transform method. This is an important concept to realistically evaluate the field variables under the coupled theory of thermoelasticity.

2. The appropriate time scale in which the effect of the inertia term is observed is considered and the importance of the inertia term is shown. When the inertia term is considered, higher values for K_I^* are achieved. The maximum value of K_I^* is about double compared to the case where the inertia term is ignored, or is not important.

3. The domain integral containing inertia term in Eq. (38) adds only more fluctuation on K_I^* variations versus time, but it has minor effect on changing the value of it.

4. Compared to the case where the inertia term is not important, strain energy has a major effect on doubling the maximum value of K_I^*.

References

[1] M.K. Kassir and A.M. Bergman, Thermal stress in a solid containing parallel circular crack. *Appl Sci Res*, **25** (1971), pp. 262–280.

[2] W.K. Wilson and I.W. Yu, The use of *J*-integral in thermal stress crack problems. *Int J Fract*, **15** (1979), pp. 377–387.

[3] H.F. Nied, Thermal shock fracture in an edge-cracked plate. *J of Therm Stresses*, **6** (1983), pp. 217–229.

[4] T.C. Chen and C.I. Weng, Coupled transient thermoelastic response in an edge-cracked plate. *Eng Fract Mech*, **39** (1991), pp. 915–925.

[5] M. Tanaka, H. Togoh and M. Kikuta, Boundary element method applied to 2-D thermoelastic problems in steady and non-steady states. *Eng Anal*, **1** (1984), pp. 13–19.

[6] V. Sladek and J. Sladek, Computation of thermal stresses in quasi-static non-stationary thermoelasticity using boundary elements. *Int J Num Meth Eng*, **28** (1989), pp. 1131–1144.

[7] V. Sladek and J. Sladek, Advanced thermoelastic analysis, L.C. Wrobel, C.A. Brebbia, Editors, *Boundary element methods in heat transfer*, Computational Mechanics Publications/Elsevier, Southampton/London (1992).

[8] S.T. Raveendra and P.K. Banedee, Boundary element analysis of cracks in thermally stressed planar structures. *Int J Solids Struct*, **29** (1992), pp. 2301–2317.

[9] P. Hosseini-Tehrani, M.R. Eslami and H.R. Daghyani, Dynamic crack analysis under coupled thermoelastic assumption. *Trans ASME J Appl Mech*, **68** (2001), pp. 584–588.

[10] F. Durbin, Numerical inversion of Laplace transforms: an efficient improvement to Dubner and Abate's method. *Comput J*, **17** (1974), pp. 371–376.

[11] G.E. Blandford, A.R. Ingraffea and J.A. Ligget, Two-dimensional stress intensity factor computations using the BEM. *Int J Numer Meth Eng*, **17** (1981), pp. 387–404.

[12] J. Martinez and J. Dominguez, On the use of quarter-point boundary elements for stress intensity factor computations. *Int. J Numer Meth Eng*, **20** 10 (1950), pp. 1941–1950.

[13] K. Kishimoto, S. Aoki and M. Sakata, Dynamic stress intensity factors using *J*-integral and finite element method. *Eng Fract Mech*, **13** (1980), pp. 387–394.

[14] S.N. Atluri, Energetic approaches and path-independent integrals in fracture mechanics, *Computational methods in the mechanics of fracture*, **vol. 2** ,in: S.N. Atluri, Editor, *Computational methods in mechanics*, North Holland, New York (1986), pp. 121–165.

[15] N.N.V. Prasad, M.H. Aliabadi and D.P. Rooke, The dual boundary element method for transient thermoplastic crack problems. *Int J Solids Struct*, **33** 19 (1996), pp. 2695–2718.

[16] P. Fedelinski, M.H. Aliabadi and D.P. Rooke, The dual boundary element method: *J*-integral for dynamic stress intensity factors. *Int J Fract*, **65** 4 (1994), pp. 369–381.

[17] D.E. Katsareas and N.K. Anifantis, On the computation of mode I and II thermal shock stress intensity factors using a boundary-only element method. *Int J Numer Meth Eng*, **38** (1995), pp. 4157–4169.

[18] B.A. Boley and J.H. Winer, Theory of thermal stresses, Wiley, New York (1960).

[19] N.D. Jadeja and T.C. Loo, Heat induced vibration of a rectangular plate. *J Eng Ind*, **96** (1974), pp. 1015–1021.

[20] K.Y. Lee and K. Sim, Thermal shock stress intensity factor By Bueckner's weight function method. *Eng Fract Mech*, **37** (1990), pp. 799–804.

[21] P. Hosseini-Tehrani, L.G. Hector, R.B. Hetnarski and M.R. Eslami, Boundary element formulation for thermal stresses during pulsed laser heating. *Trans ASME J Appl Mech*, **68** (2001), pp. 480–489.

Corresponding author. Tel.: +98 21 7391 3972; fax: +98 21 7491 225.

Home   Browse   Search   My settings   My alerts   Shopping cart

About ScienceDirect
What is ScienceDirect
Content details
Set up
How to use
Subscriptions

Contact and Support
Contact and Support

About Elsevier
About Elsevier
About SciVerse
About SciVal
Terms and Conditions
Privacy policy